10 Metal-Oxide Superconductors

Metal-oxide superconductors commonly base on a perovskite-type structure. The standard perovskite $BaTiO_3$ forms a body-centered cubic structure with Ba at the body-centered position, Ti at the corners of a cube and O at the edge-centered positions. This structure can be regarded as stack of Ti-O and Ca-O layers as well. Starting from this structure a vast of superconductors have been synthesized or even designed by replacing the *d* metal ion, doping on the Ba site, doubling the unit cell in one direction, inserting additional *d* metal ion-oxygen layers, tuning the charge-carrier concentration, e. g. by changing the oxygen stoichiometry, or all changes together. In this way, supercells with ordered stacking sequences along the *c* direction have created which become superconducting at temperatures up to 133 K, as for example in $HgBa_2Ca_2Cu_3O_{8+\delta}$ [1]. $HgBa_2Ca_2Cu_3O_{8+\delta}$ has a sandwich structure consisting of three CuO_2 layers separated by Ca layers and embedded in a roll made of a Hg/Ba-O double layers. A common feature of most metal-oxide superconductors is the *d* metal ion-oxygen layer as a building block and its subtle influence on the electronic properties. Very often a strongly two-dimensional metal is observed with conductivity (and superconductivity) mainly within these layers.

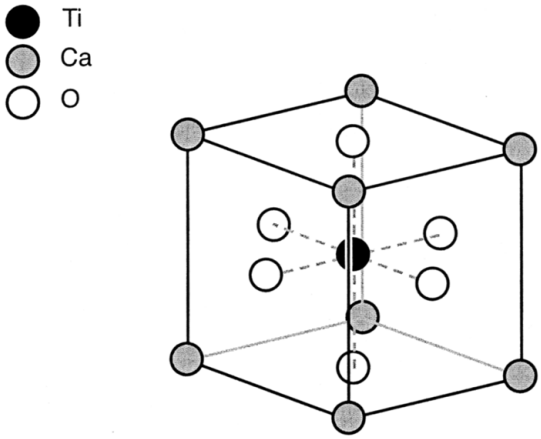

Fig. 10.1. Crystal structure of the perovskite $CaTiO_3$, the main structure element of the high-temperature superconductors (from [2]). It corresponds to the standard perovskite $BaTiO_3$ unit cell shifted along the [111] direction by (1/2, 1/2, 1/2)

G. Goll: *Unconventional Superconductors*
STMP **214**, 121–151 (2006)

10.1 Sr_2RuO_4

Sr_2RuO_4 belongs to a perovskite-related layered series, the so-called Ruddlesden-Popper series $Sr_{m+2}Ru_{m+1}O_{3m+4}$ where the d metal site is occupied by Ru. Sr_2RuO_4 is one example of this general structure with $m = 0$ and one RuO_2 layer. There exist two further members of this series $Sr_3Ru_2O_7$ ($m = 1$) and $SrRuO_3$ ($m = \infty$), which are non-superconducting, but exhibit strongly ferromagnetic correlations. $SrRuO_3$ is an itinerant $4d$ ferromagnet with a Curie temperature $T_c \approx 160\,\mathrm{K}$ [3, 4] and $Sr_3Ru_2O_7$ a metamagnet with strong critical fluctuations [5]. The structure of Sr_2RuO_4 is closely related to the high-temperature superconductor $(La,Sr)_2CuO_4$ with Cu replaced by Ru (see Fig. 10.2), but superconductivity appears only below $T_c \leq 1.5\,\mathrm{K}$.

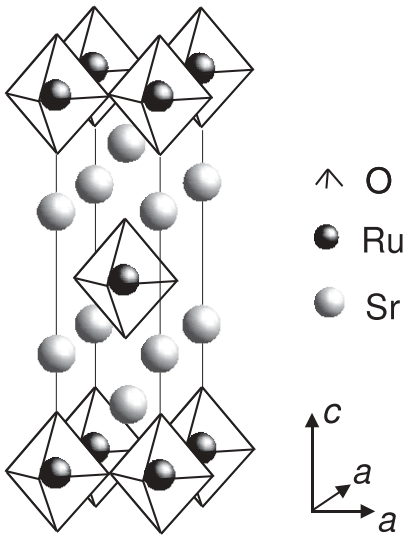

Fig. 10.2. Crystal structure of Sr_2RuO_4 which crystallizes in a K_2NiF_4-type structure belonging the tetragonal space group $I4/mmm$

The discovery of superconductivity in Sr_2RuO_4 has quickly triggered a large amount of interest because of the unconventional properties [6] and the initially proposed analogy [7] to ^{3}He. The normal state of Sr_2RuO_4 is well described by Fermi liquid theory with strong correlation effects which enhance the effective mass seen in quantum oscillation [8, 9], specific heat and Pauli spin susceptibility measurements[1]. The quasi-two-dimensional Fermi surface consists of three weakly corrugated sheets, the hole-like α band, and the electron-like β and γ bands, which can be mainly associated with three t_{2g} orbitals of Ru [9]. A major source of complications arises from the presence of four electrons in three nearly degenerate Ru orbitals

[1] For a review of the normal-state properties see [10].

$4d_{xy}$, $4d_{yz}$, and $4d_{xz}$ and the competing effects of crystal field, spin-orbit interaction and Hund's coupling. In the normal state orbital dependent, predominantly ferromagnetic spin correlations have been reported by NMR experiments [11], but neutron scattering did not detect ferromagnetic correlations so far, which would help to explain a spin-triplet superconducting state in a simple picture. In fact, incommensurable antiferromagnetic fluctuations above [12] and below [13] T_c are reported by neutron scattering with a strong fluctuation amplitude at $\boldsymbol{q} \approx (0.6\pi, 0.6\pi)$. The fluctuations are due to nesting of the α and β sheets which had been predicted independently by Mazin and Singh [14]. This suggests a subtle competition between ferro- and antiferromagnetic spin correlations and the role of these spin fluctuations for the pairing mechanism is still a matter of an ongoing debate.

The superconducting state is extremely sensitive to impurities and disorder. Systematic doping of nonmagnetic Ti on the Ru site increases the residual resistivity ρ_{ab} above $\approx 1\,\mu\Omega$cm for $x > 10^{-3}$ and immediately suppresses superconductivity [15, 16]. This is in line with earlier observations [17, 18] that defects or impurities both rapidly suppress superconductivity, if the residual resistivity is increased above $\approx 1\,\mu\Omega$cm. The extreme sensitivity of T_c to nonmagnetic impurities is consistent with pair-breaking in unconventional superconductors and has been observed in the unconventional superconductor UPt_3 [19] and the high-T_c cuprates [20] as well. The suppression can be modelled by a generalized Abrikosov-Gor'kov pair-breaking theory [21] adapted for nonmagnetic impurities in a superconductor with an unconventional gap symmetry [22, 23].

The exact symmetry of the superconducting order parameter of Sr_2RuO_4 [24, 25, 26, 27, 28, 29] and notably the pairing mechanism [12, 14, 30, 31, 32] are still controversial as well. On the base of the later discussed experiments several models for the superconductivity in Sr_2RuO_4 have been developed and adapted according to the experimental progress. These models will be discussed at the end of the section after a short description of the experimental situation[2].

Nodal Structure

Early measurements [34] showed a large residual specific heat for $T \to 0$ which prevent from a definite assignment of the low-T temperature dependence. Due to an improved sample quality the residual specific-heat contributions were significantly reduced. From measurements on samples with T_c ranging from 0.43 K to 1.17 K [35] it is expected , that no residual contribution remains for samples with optimal T_c, i. e. that the residual specific heat is not intrinsic. The specific heat data on the best crystals reveal a T^2 dependence at $T < T_c/2$ probably caused by line nodes of the energy gap. In addition, the jump ΔC at T_c is much smaller than that expected from an isotropic gap. One finds $\Delta C/\gamma T_c = 0.74$ in line with the low-temperature behaviour.

The angular dependence of the specific heat on the applied magnetic field orientation was used as a probe for the quasiparticle density of states induced by the

[2] A more extended review of the superconducting properties was given by Mackenzie and Maeno [33] (on the basis of the knowledge in spring 2002)

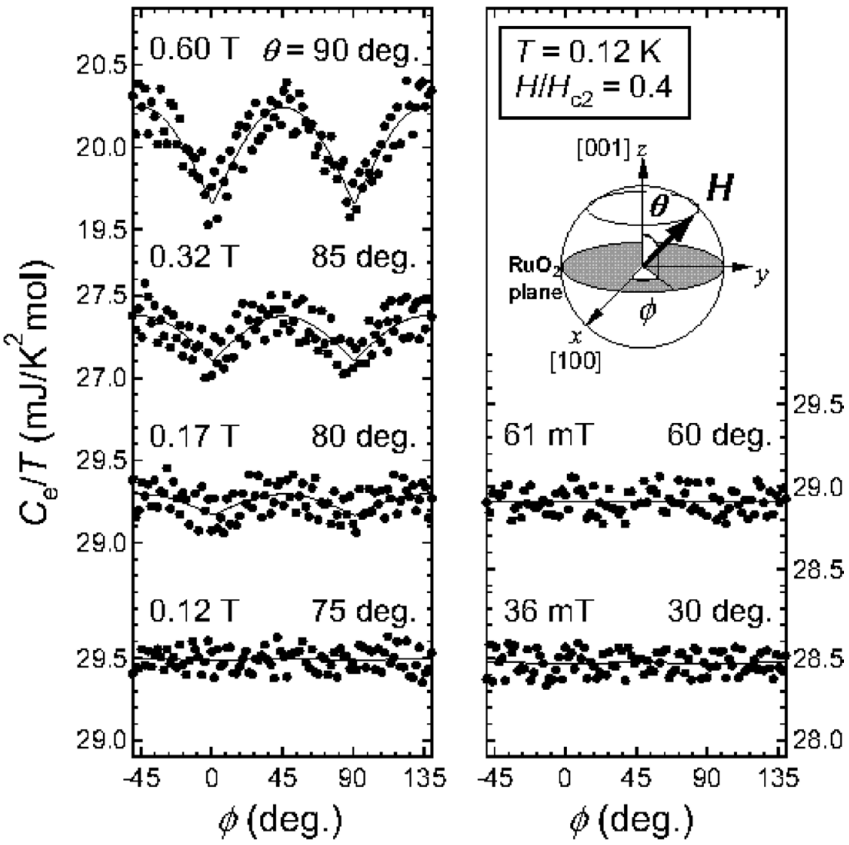

Fig. 10.3. Field-orientation dependent specific heat C_e/T measured by rotating the applied magnetic field on a cone with polar angle Θ. ϕ is the azimuth angle and the measurements have been done at fixed $T = 0.12\,\mathrm{K}$ and reduced magnetic field $H/H_{c2} = 0.4$. For details see text (from [36])

magnetic field. An oscillatory modulation of the thermodynamic quantities has theoretically been predicted by Vekhter et al. [37] and Won and Maki [38, 39] for the vortex state of d-wave superconductors. The observed in-plane anisotropy (see Fig. 10.3 for $\Theta = 90°$ ($H \perp c$)) below 0.3 K which is absent in the normal state has been interpreted as a modulation of the superconducting gap on the γ band with a minimum along the [100] direction [40]. For the field range $0.15\,\mathrm{T} < \mu_0 H < 1.2\,\mathrm{T}$ the non-sinusoidal 4-fold angular variation can be approximated by

$$C_e(\phi) = C_0 + C_4 \cdot f_4(\phi) \tag{10.1}$$

with $f_4(\phi) = 2|\sin 2\phi| - 1$. Further studies extended to smaller polar angles show a steeply decrease of $C_4(\phi)$ with decreasing Θ from 90° (i. e. towards $H \parallel c$). No angular modulation of $C_e(\phi)$ was detected below $\Theta = 80°$ (see Fig. 10.3). Deguchi et al. concluded that the origin of this behaviour is the compensation by gap anisotropy in

the α and β bands which most probably have line nodes or gap minima along [110], i. e. with antiphase with that of the γ band [36][3].

Further hints at the nodal structure were obtained from thermal conductivity measurements. Zero-field experiments on single crystal with $T_c = 1.44\,\mathrm{K}$ show a quadratic temperature dependence of κ below T_c down to $\approx 0.3\,\mathrm{K}$ and a residual κ/T which is independent of T_c, i. e. of the impurity concentration [41, 42, 43, 44]. Furthermore, below $T \approx 0.3\,\mathrm{K}$ samples with a high T_c show an crossover to a T^3 dependence of κ [43] signalling the crossover from heat transport dominated by the quasiparticle excitations at the nodes to heat transport dominated by bound states. Both, the residual and the T^3 contributions, have been discussed in the context of various models and it appears that the residual term is compatible with the universal limit of κ/T [45]. The T^3 dependence has been predicted by Zhitormirsky and Walker [46] and Graf and Balatsky [26] for the orbital dependent gap structure and scattering in the unitary limit.

In an applied magnetic field the thermal conductivity increases linearly with field [41, 47]. It has been shown that this is consistent with $\kappa(H)$ in very clean superconductors with line nodes. In addition, Izawa et al. [41] rotated the magnetic field within the RuO_2 plane and observed contributions with two- and fourfold symmetry of the in-plane thermal conductivity. In comparison with various proposals for the gap function they conclude that both contributions are incompatible with any model with vertical line nodes, but strongly indicate the presence of horizontal line nodes.

Hints at line nodes of the gap function came from the temperature dependence of the penetration depth λ as well. Bonalde et al. [48] reported on penetration-depth measurements on Sr_2RuO_4 single crystals of different quality utilizing a 28 MHz tunnel diode oscillator. Samples with a rather high T_c close to 1.4 K unanimously exhibit a T^2 dependence below 0.8 K down to 40 mK. In contrast, a dirty sample with $T_c = 0.82\,\mathrm{K}$ shows $\Delta\lambda(T) = \lambda(T) - \lambda(0.04\,\mathrm{K}) \propto T^3$ below 0.6 K. These power laws have been discussed in the framework of several models including the orbital-dependent superconductivity model [49], an anisotropic p-wave model [50] and a weak-coupling d-wave model in order to account for possible line nodes. Only the gap function with line nodes reproduces the quadratic temperature dependence at low temperatures satisfactory, if, in addition, the presence of impurities is taken into account. However, no crossover to a linear behaviour has been found as expected from the local-limit calculations by Hirschfeld and Goldenfeld [51]. The observation of a T^3 dependence of $\Delta\lambda$ in the sample with lower T_c instead of a more pronounced T^2 dependence lead to the conclusion, that nonlocal effects might be responsible for the observed exponents. According to Kosztin and Leggett [52] nonlocal electrodynamics in superconductors with line nodes of the order parameter can cause a quadratic T dependence instead of a linear T dependence even in the clean limit. In the presence of impurities (dirty nonlocal limit) a T^3 dependence would be expected [52] at low temperatures. Recently, Kusunose and Sigrist [28] showed that the orbital-dependent superconductivity model in the clean nonlocal limit allows a consistent description of the experimental data of Bonalde et al. [48] as well.

[3] The underlying order-parameter scenario is discussed later at the end of this section.

Penetration-depth measurements by μSR experiments in the transverse field have been performed only on samples with rather low $T_c \simeq 0.7\,\mathrm{K}$ [53] and $T_c \simeq 1.15\,\mathrm{K}$ [54]. From the real part of the Fourier transform of the time evolution of the muon polarization the probability distribution of the local fields and its width $\langle \Delta B^2 \rangle^{1/2} \propto \lambda^{-2}$ was determined. A closer inspection of the temperature dependence yields

$$\lambda_{ab}^{-2}(T) = \lambda_{ab}^{-2}(0)(1 - (T/T_c)^{\alpha}) \tag{10.2}$$

with $\lambda_{ab}(0) = 200 \pm 20\,\mathrm{nm}$ [53] and $\lambda_{ab}(0) = 190\,\mathrm{nm}$ [54]. Both experiments yield $n = 2.5$ [53] and $n = 2.78$ [54] for the exponent α which is close to the BCS expectation (see discussion in Sect. 4.3). This would imply a nodeless energy gap of s- or p-wave symmetry. However, at low temperature the data in [53] are also consistent with a linear temperature dependence which is usually taken as an indication of the presence of nodes. For a definite conclusion one has to await measurements on samples with higher T_c where impurities do not mask the intrinsic temperature dependence.

A non-exponential T dependence has also been reported from ultrasound attenuation measurements [57, 56]. While Matsui and coworkers reported a crossover from T^2 to T^3 behaviour above $\approx 0.4\,\mathrm{K}$ for the transverse sound attenuation (see also comment by Gavenda [58]), Lupien et al. [56] investigated the longitudinal and transverse ultrasound attenuation in the normal and superconducting states with sound propagating along the $\langle 100 \rangle$ and $\langle 110 \rangle$ direction in the basal plane and found both a significant anisotropy and power-law behaviour down to $T_c/30$. The data have been analyzed by Walker et al. in a model where the ultrasound attenuation is determined by the electron-phonon matrix element [55] (see Sect. 3.3). They showed that the strong anisotropy of the ultrasound attenuation is connected with the layered square-lattice structure of Sr_2RuO_4 and occurs only in the interaction of phonons with electrons in the γ band, but not with electrons in the α and β bands. Therefore, the attenuation of the most strongly attenuated modes is associated with their interaction with the electrons in the γ band and thus gives information about the nodal structure of this band, while the attenuation of the most weakly attenuated modes probes the nodal structure of the α and β bands. Under the assumption of an order parameter that transforms as the E_u irreducible representation of the point group D_{4h} and parametrized by

$$\boldsymbol{d}^i(\boldsymbol{k}) = \sum_n \boldsymbol{d}_n^i e^{\imath \boldsymbol{k} \boldsymbol{R}_n} \tag{10.3}$$

with

$$\boldsymbol{d}_x^i(\boldsymbol{k}) = \delta^i \sin(k_x a) + \sin\left(\frac{k_x a}{2}\right)\cos\left(\frac{k_y a}{2}\right)\cos\left(\frac{k_z c}{2}\right) \tag{10.4}$$

and

$$\boldsymbol{d}_y^i(\boldsymbol{k}) = \delta^i \sin(k_y a) + \cos\left(\frac{k_x a}{2}\right)\sin\left(\frac{k_y a}{2}\right)\cos\left(\frac{k_z c}{2}\right) \tag{10.5}$$

where $i = \alpha, \beta, \gamma$ denotes the band index, they achieved a quantitative description of the data (see Fig. 10.4). The best fits were obtained with $\Delta_0^{\gamma} = 0.7\,\mathrm{meV}$ and

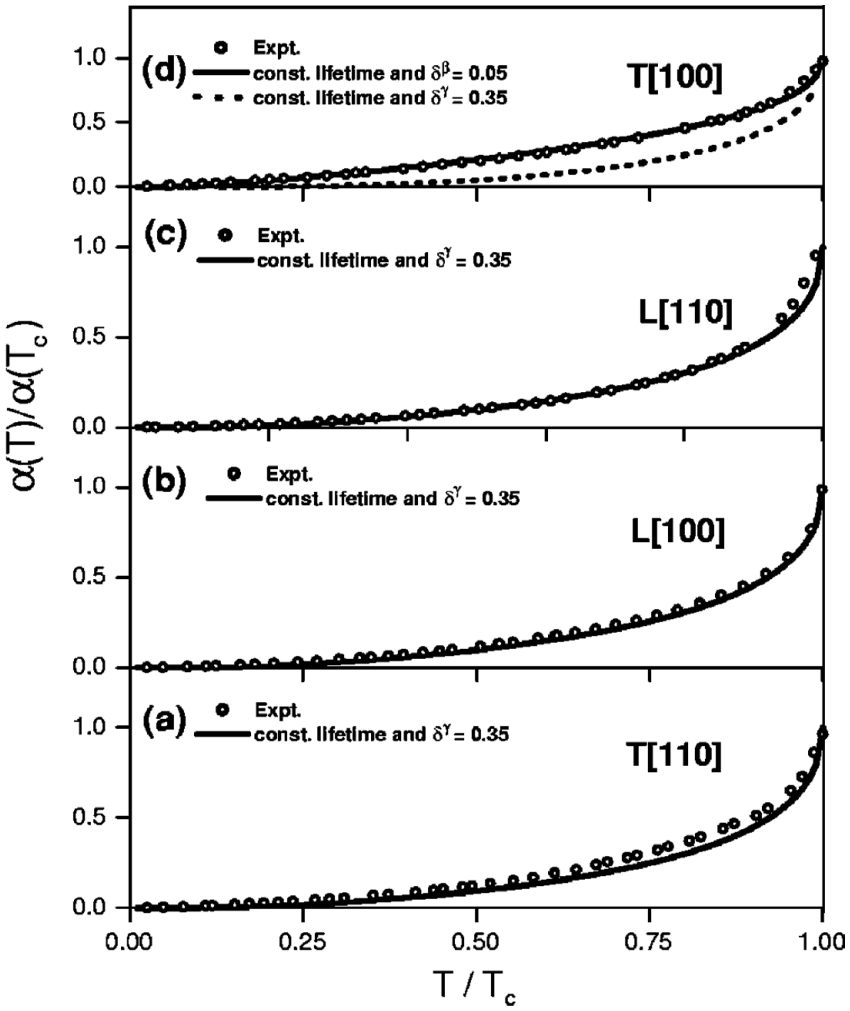

Fig. 10.4. Numerical fits of the temperature dependence of the in-plane ultrasound attenuation modes of Sr_2RuO_4 (from [55]). The free parameters are δ^γ and Δ_0^γ (for explanation see text). The exerimental data have been published by Lupien et al. [56]

$\delta^\gamma = 0.35$. The non-zero δ indicates that the horizontal line node at $k_z = \pm\pi/c$ ($\delta^i = 0$) is removed and point nodes appear instead.

Parity and Spin State

One of the early hints at unconventional superconductivity in Sr_2RuO_4 came from zero-field muon-spin relaxation measurements that reveal the spontaneous appearance of an internal magnetic field below the transition temperature [59]. As already discussed, the appearance of such a field indicates that the superconducting state is

characterized by the breaking of time-reversal symmetry. This spontaneous internal magnetic field can be caused either by a finite hyperfine field or spontaneous supercurrents in the vicinity of inhomogeneities in the order parameter near impurities, surfaces and/or domain walls [60, 61]. The knowledge of the origin would help to discriminate between unitary and non-unitary states. However, this distinction cannot be made from the μSR results. From the increase in the exponential relaxation below T_c a characteristic field strength of 0.5 G was estimated. This is about the same as observed in the B phase of UPt_3 [62].

NMR/NQR measurements on Sr_2RuO_4 benefit from the presence of three possible local probes within the RuO_2 plane, namely the natural abundant Ru isotopes ^{99}Ru and ^{101}Ru both with nuclear spin $I = 5/2$ and the O isotope ^{17}O with $I = 1/2$ which has to replace the natural ^{16}O without nuclear spin. Therefore, the Knight shift and the nuclear relaxation rate can be measured on different local sites. As already mentioned in Sect. 4.2 the Knight shift reveals information on the spin state in the superconducting state. Both ^{17}O [63] and ^{99}Ru [64] Knight shift measurements with magnetic field applied perpendicular to the c axis, i. e. within the RuO_2 planes, indicate an unchanged spin susceptibility below T_c which identifies Sr_2RuO_4 as a spin-triplet superconductor. The result reinforces that the electrons in Sr_2RuO_4 are bound together in parallel-spin pairs parallel to the RuO_2 plane, consistent with a vector order parameter $\boldsymbol{d}(\boldsymbol{k})$ pointing along the c axis. Measurements of the ^{101}*Ru*-Knight shift in a magnetic field parallel to the c axis (see Fig. 10.5) also find an invariance of the Knight shift with respect to the field and temperature on passing through the upper critical field and T_c, respectively, if the applied field is larger than 200 Oe [65]. This finding was interpreted in a scenario where the $\boldsymbol{d}$ vector pointing to the c axis in zero field can flip perpendicular to the c axis by application of a small magnetic field along c.

The absence of a Hebel-Slichter peak in the nuclear relaxation rate $1/T_1$ on both sites was taken as a first sign of non-s-wave superconductivity in Sr_2RuO_4. Further, the temperature dependence of the nuclear relaxation rate yields information on the nodal structure. While early measurements of the ^{101}Ru relaxation rate on a sample with rather low $T_c = 0.7$ K found a linear T dependence [66], subsequent experiments on samples with T_c close to 1.5 K showed a T^3 power law of $(1/T_1)^{^{101}\mathrm{Ru}}_{\mathrm{NQR}}$ down to 0.15 K. The T^3 dependence is an indication of the gap function with line nodes. Consequently, the T-linear behaviour was ascribed to impurity effects. The observation of a T^3 dependence has been used for a comparison of various models for the superconductivity in Sr_2RuO_4. The result favors a p-wave model with a strongly anisotropic gap [50] or with a line node [67]. In contrast, the nuclear relaxation rate $(1/T_1)^{^{17}\mathrm{O}}_{\mathrm{NQR}}$ on the ^{17}O site shows a T-linear behaviour even for high-T_c samples in zero field [68]. Application of a magnetic field parallel to the planes completely suppresses the linear T dependence at low T. This was interpreted as an emergence of gapless thermal spin fluctuations for the out-of-plane component along the c axis which possibly originate from the thermal motion of the domain structure of a superconducting $k_x \pm ik_y$ state.

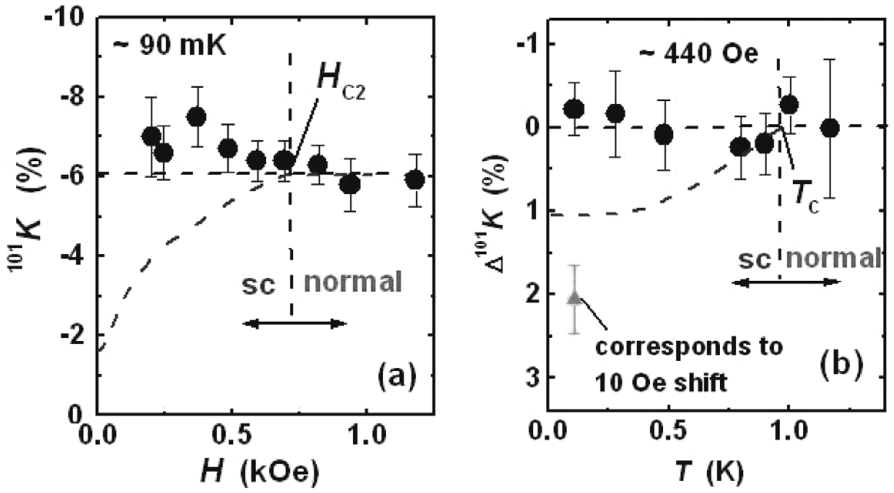

Fig. 10.5. Magnetic-field (**a**) and temperature dependence (**b**) of the ^{101}Ru-Knight shift in a field applied parallel to the c axis of Sr_2RuO_4 (by courtesy of K. Ishida, U Kyoto)

Energy Gap

Information on the energy-gap size and symmetry have been obtained from several experiments. While Laube et al. [69] investigated point contacts between Sr_2RuO_4 and a sharpened Pt needle as a normal metal counterelectrode, Jin et al. [70] used planar Pb-Sr_2RuO_4 tunnel junctions, and Upward et al. [71] vacuum tunnelling spectroscopy between a Pt/Ir tip and a cleaved Sr_2RuO_4 surface. The planar tunnelling measurements reveal the presence of an insulating surface layer of unknown origin. The tunnelling characteristics of the Pb-Sr_2RuO_4 junction show a clear gap feature, but resembles very much the tunnelling characteristics of superconducting Pb with $\Delta_{Pb} = 1.4$ meV in accordance with the literature value of $2\Delta_{Pb}/k_BT_c = 4.3$ [72]. No further gap structure is observed (see Fig. 10.6), although, features from both superconductors should be present in the tunnelling characteristic of a superconductor-superconductor tunnel junction. This hints at a strong surface degradation of Sr_2RuO_4 during the preparation process.

The vacuum tunnelling data reveal a much smaller width of the relevant features in the tunnelling spectra (see Fig. 10.7). Similar tunnelling characteristics have been obtained irrespectively of the position of the Pt/Ir tip on different crystals or at different locations of the same Sr_2RuO_4 crystal and the characteristic features disappear above T_c. The authors interpreted the maxima at finite bias as a manifestation of the singularity in the density of states expected at Δ_{max} and determined Δ_{max} from the position of this maxima. They derived a BCS parameter $2\Delta_{max}/k_BT_c = 6.2 - 8$ and accounted the enhanced value to a large gap anisotropy as arising e. g. from vertical line nodes.

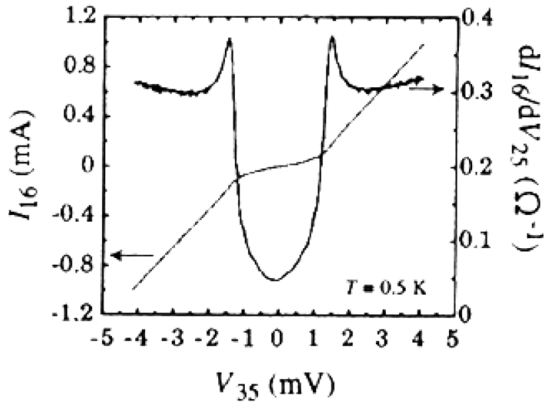

Fig. 10.6. Tunneling characteristic for a Pb-Sr_2RuO_4 tunnel junction along the c axis at T = 0.5 K (from [70])

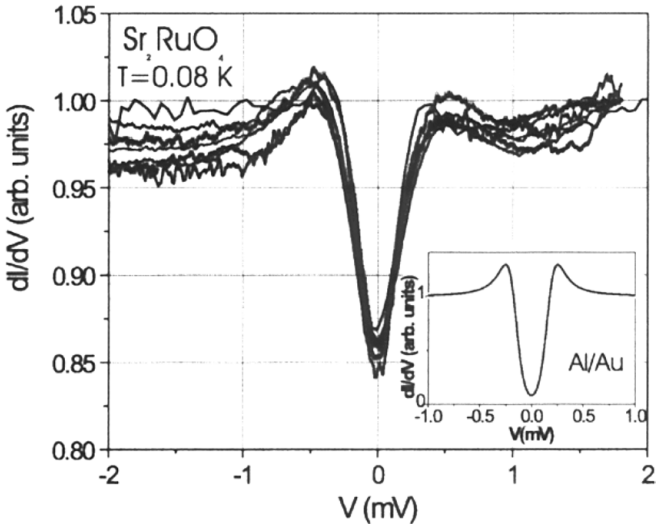

Fig. 10.7. Tunneling spectra on different crystal or at different locations of the same Sr_2RuO_4 crystal at T = 0.08 K (from [71])

The point-contact measurements were performed on two single crystals, grown both by a floating zone technique in different groups[4]. Determination of T_c was carried out via bulk resistivity measurements. A total of about 150 contacts have been investigated with contact resistances typically ranging from R_0 = 0.5 to 25 Ω.

[4] Crystal #5 was provided by F. Lichtenberg at Augsburg University and shows a midpoint transition temperature $T_c^{50\%}$ = 1.02 K with a transition width $\Delta T_c^{90\%-10\%}$ = 0.035 K, crystal #C85B5 was grown by Z. Q. Mao and Y. Maeno at Kyoto University and has $T_c^{50\%}$ = 1.54 K and $\Delta T_c^{90\%-10\%}$ = 0.15 K.

The measurements were performed in different configurations of the predominant current injection relative to the crystallographic axis of Sr_2RuO_4 and the applied magnetic field. In addition, the influence of the surface treatment has been investigated.

Spectroscopic information was obtained only from contacts with current injection parallel to the *ab*-planes because the transport through such contacts was in the ballistic limit. In the spectra with current perpendicular to the *ab*-planes evidence for non-spectroscopic effects have been found [73]. These have been explained in terms of the heating model [74] for contacts in the thermal limit (see Sect. 5.3). For both crystals two distinctly different types of structures in dV/dI vs V spectra are observed in the superconducting state: either a double-minimum structure (curve 1 and 2 in Fig. 10.8) or a zero-bias anomaly, i. e. a single-minimum structure centered

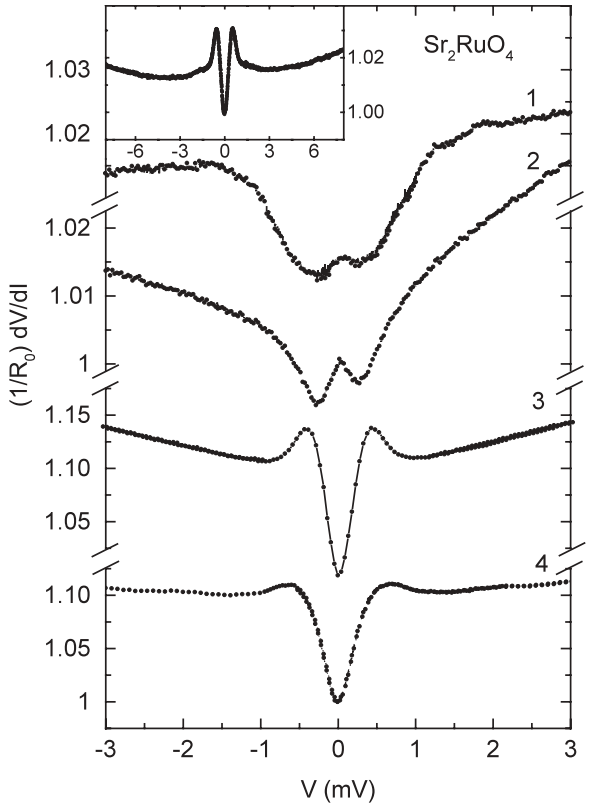

Fig. 10.8. Differential resistance dV/dI vs bias voltage V normalized to the zero-bias resistance R_0 measured at low $T = 0.2\,\mathrm{K} \ll T_c$ with $R_0 = 4.4$ (curve 1), 5.0 (2), 5.3 (3), and $3.6\,\Omega$ (4). The inset shows a dV/dI curve with $R_0 = 7.6\,\Omega$ to higher bias. Note that the differential resistance dV/dI and not the differential conductance dI/dV is shown, therefore, the zero-bias anomaly in curve 3 and 4 appears as a minimum and not as a maximum

at $V = 0$ (curve 3 and 4 in Fig. 10.8). These structures appear independently of the contact resistance and the in-plane orientation of the current. The occurrence of a zero-bias anomaly is believed to have its origin in an Andreev-bound surface state hinting at an unconventional order parameter of the superconducting phase which changes sign as function of the **k**-vector. The shape of the spectra were satisfactorily reproduced by an analysis of the data in terms of a p-wave pairing state with order parameter $\mathbf{d}(\mathbf{k}) = \hat{\mathbf{z}}(k_x \pm ik_y)$. The current transport across the contact was modelled allowing a tunable transparency and a phenomenological acceptance cone. Within this model, amongst other things, information about the transmittivity of the contact has been extracted [69]. Contacts showing the zero-bias anomaly are described by a low transmission probability, the ones with double-minimum structures are described by a high transmission probability.

The temperature dependence of both types of spectra is shown in Fig. 10.9a and b, together with the calculated spectra. In both cases, the structures related to superconductivity become weaker with increasing temperature and vanish near T_c. The temperature dependence of the theoretical curves were calculated without additional parameter once Δ_0 has been determined by fitting to the spectrum at lowest T. Identical values for $\Delta_0 = 1.1$ meV have been extracted from both types of spectra, which is about 5 times the value expected from a weak-coupling theory.

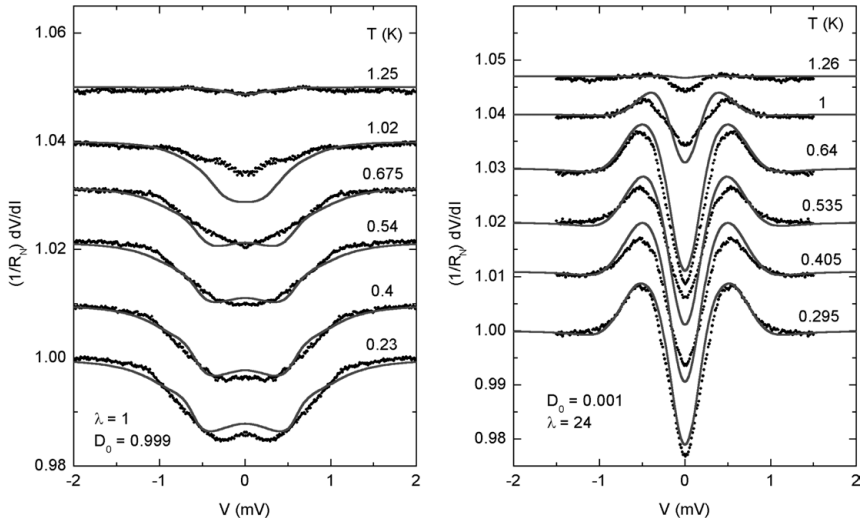

Fig. 10.9. Temperature dependence of the spectra with a double-minimum structure (**a**) or with a single-minimum (**b**). Closed (open) symbols denote the measured (calculated) spectra. For clarity, the curves at higher T are shifted with respect to the curve at lowest T. D_0 is the transmission probability for quasiparticles along the contact normal and λ is a measure for the opening angle of the acceptance cone

Point contacts of high transmission exhibit a direct metallic conductivity, and, in contrast to the tunnelling limit, excess current I_{exc} occurs. This additional current through the constriction is a consequence of the Andreev scattering process and carries further information on the order parameter (see Sect. 5.3). For classical superconductors with an isotropic energy gap Δ the excess current is proportional to Δ [75]. From the proportionality it follows that both quantities exhibit the same functional dependence on temperature and magnetic field, respectively. For unconventional superconductors, however, this relation is altered in the presence of impurities and the excess current is not necessarily proportional to the order parameter. Experimentally, a strikingly linear dependence of the excess current as a function of temperature and applied magnetic fields over a surprisingly wide range of the phase diagram has been obtained (see Fig. 10.10). Each symbol in the lower panel represents one point contact either on sample #5 (open symbols) or #C85B5 (filled symbols). The excess current was determined by numerical integration of dI/dV vs. V after subtraction of a normalconducting background. The normalization values $I_{\mathrm{exc}}^{\mathrm{fit}}(H = 0)$ and $H^{\mathrm{fit}}(I_{\mathrm{exc}} = 0)$ have been determined from linear regression of the $I_{\mathrm{exc}}(H)$ vs. H data for each point contact separately. The inset shows typical dI/dV curves from which the excess current was derived. Note that the result is quite universal since it is found in both samples in spite of their different value of T_c. As outlined by Laube et al., the observed equivalence of the linearity in the field and temperature dependence implies a well defined functional dependence of the excess current I_{exc} on the superconducting gap Δ. In general, one obtains a scaling relation $I_{\mathrm{exc}} = \text{constant} \times \Delta^{1/\nu}$ close to T_c, where ν is defined by the order-parameter symmetry [76].

These observations have been discussed in the framework of the p-wave triplet pairing state [24, 25] in the presence of impurities. The pairing state can qualitatively account for the linear behaviour of the excess current. The p-wave analysis to the point-contact spectra [69] yields the BCS temperature dependence for the superconducting gap in Sr_2RuO_4, i.e., $\nu = 0.5$ (thin full line in Fig. 10.10 upper panel). The resulting temperature dependence of the excess current determined in the framework of the p-wave analysis is shown in Fig. 10.10 as $I_{\mathrm{exc},1}$ (diamonds). The calculations are performed for a mean free path of 15 coherence lengths ($\xi_0 = v_f/2\pi T_c$) and for a diffusively scattering surface. It is clear that this model is insufficient to describe the experimental data (squares). This is also true for the overall magnitude of the bulk gap $\Delta(0) = 1.1\,\mathrm{meV} = 5.6 \times 1.76 k_{\mathrm{B}} T_c$. The general conclusion, however, is that unlike in the s-wave case in unconventional superconductors the excess current is not necessarily proportional to the order parameter. This is a result of the fact that impurities and disorder strongly affect the surface properties of unconventional superconductors. To reconcile the measured $\Delta(0)$ and $I_{\mathrm{exc}}(T)$ with a p-wave order parameter an additional pair-breaking channel has to be considered. It was shown by Millis et. al. [22] that a low-frequency bosonic mode at a characteristic frequency ω_p described by an Einstein spectrum $A_p(\omega) = \frac{\pi}{2} J_p \omega_p \delta(\omega - \omega_p)$ leads to a *temperature dependent* pair-breaking parameter

$$\Gamma_{\mathrm{in}}(T) = \frac{(1-g)}{4} J_p \omega_p \coth\left(\frac{\omega_p}{2T}\right), \tag{10.6}$$

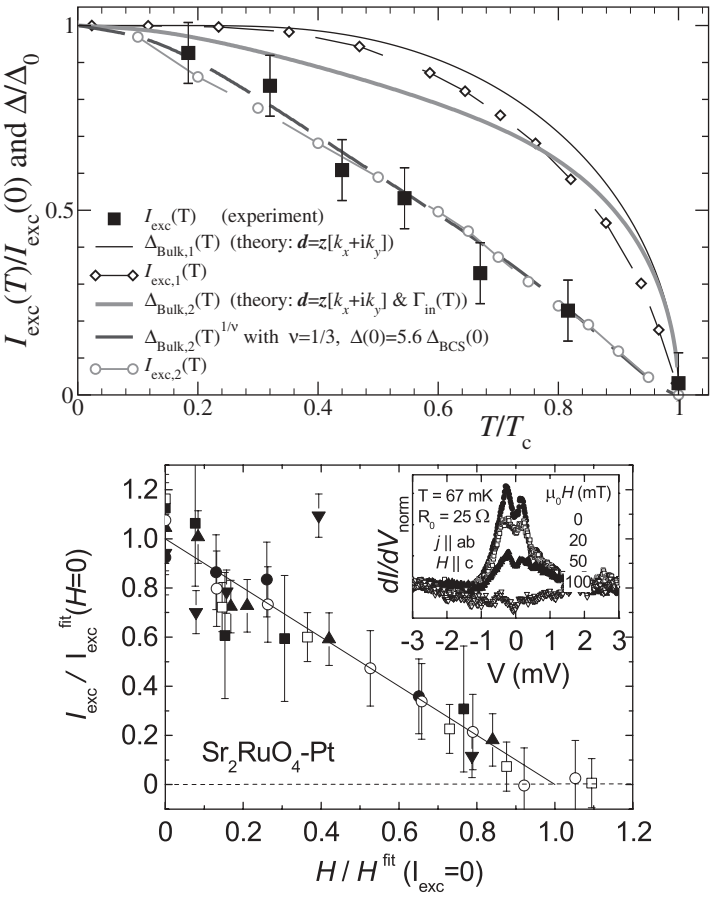

Fig. 10.10. *Upper panel*: Temperature dependence of the normalized excess current across a point contact in Sr_2RuO_4. Experimental results (*squares*) and the results of the calculation (*open symbols*) for the excess current from a p-wave analysis are shown, without (*diamonds*) and with (*circles*) the effect of an inelastic scattering channel $\Gamma_{in}(T)$. The dashed thick curve illustrates the scaling relation $I_{exc,2}(T) \sim \Delta_{bulk,2}(T)^{1/\nu}$ for the inelastic scattering
Lower panel: Field dependence of the normalized excess current across several point contacts in Sr_2RuO_4. The magnetic field H is aligned almost parallel to the c-axis, and the current accross the point contact is applied in the *ab*-plane. Each symbol represents one point contact on one of the two studied samples. The full line is a guide to the eye. For explanation of $I_{exc}^{fit}(H = 0)$ and $H^{fit}(I_{exc} = 0)$ see text. The inset shows for one point contact typical dI/dV curves from which the excess current was determined as a function of magnetic field

where g is the coupling-constant appearing in the gap equation. For the excess current this model gives an excellent agreement with experimental data, as shown by $I_{exc,2}$ (circles) in Fig. 10.10 for $\omega_p = 0.5T_c$ and $\frac{(1-g)}{4} J_p = 2\pi \times 0.25$.

Field-dependent calculations near H_{c2} are complicated due to the presence of vortices near the interface, and have not been performed within the *p*-wave approach so far. However, from experiment it is obvious that with increasing magnetic field both types of structures are weakened until they vanish close to B_{c2}. In addition to the structures attributed to superconductivity, a maximum in the spectra centered at $V = 0$ starts to develop - already below B_{c2} - and becomes more pronounced with increasing field. The maximum is observed in a wide range of the (B, T) diagram and persists even above T_c up to several K. The maximum in dV/dI signals insulating behaviour, but its origin is not yet understood. Several scenarios, including magnetic or Kondo-type origin, a lattice distortion at the surface or a structural instability of Sr_2RuO_4, have been discussed [77]. A field-induced structural instability at the surface seems the most promising candidate, but further work is necessary for a definite assignment. For example, scanning tunnelling microscopy in an applied magnetic field can be helpful for a clarification.

Phase-Sensitive Measurements

Several experiments have been performed on Sr_2RuO_4 by different groups [70, 78, 79, 80, 81] in order to study the pairing symmetry and to obtain a doubtless confirmation of the proposed order-parameter symmetry. However, despite of the experimental efforts, the situation is still contradictory. This has mainly to do with difficulties in preparing reliable and uniform Josephson junctions. Although pair tunnelling was achieved in most junctions, none of the junctions show a clear Fraunhofer pattern of the critical current as a function of applied magnetic field which hints at spatial fluctuation of the critical supercurrent density.

A reduction of the critical current between two Pb electrodes was observed in a Pb/Sr_2RuO_4/Pb junction (see Fig. 10.11a) when it was cooled below the critical temperature of Sr_2RuO_4 [70]. In SN′S type junctions a weakening of the coupling between two *s*-wave electrodes is expected, if the interlayer N′ becomes superconducting with non-*s*-wave pairing symmetry [82]. However, this experiment both benefits and suffers from the presence of Ru lamellas in the junction region

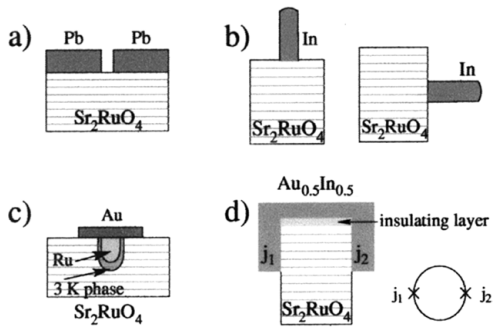

Fig. 10.11. Several examples of junctions on Sr_2RuO_4 for studies of the pairing symmetry (from [81])

(see Fig. 10.11c). It benefits, because proximity-induced coupling between Pb and Sr_2RuO_4 occurs probably only due to the presence of these inclusions, which open a "window" through the insulating surface layer on Sr_2RuO_4 and it suffers from it, because the influence of the lamellas on the pairing symmetry in the junction region is elusive. Nevertheless, the result at least points to a non-*s*-wave pairing symmetry of Sr_2RuO_4.

Jin et al. [79] prepared a SS′ type Josephson junction by pressing an Indium wire against the sample surface and observed a orientation-dependent Josephson current. A supercurrent was present for in-plane junctions or absent for junctions along the *c* axis (see Fig. 10.11b). This result was interpreted as an indication for an order parameter with either *p*- or *d*- wave symmetry. The directional dependence of the supercurrent arises from a directional dependence of spin-orbit coupling strength which is responsible for a mixing between *s*- and *p*-wave pairs and thereby enables Josephson coupling (see Sect. 6.1).

Sumiyama et al. [78] prepared SS′ type junctions by evaporating Nb or Sn through a shadow mask on a pre-structured Sr_2RuO_4 surface (see Fig. 10.12). No directional dependence of the supercurrent was observed, for both orientations of the crystal a Josephson coupling was reported. The reason for the discrepancy between both experiments is not clear. As possible origins the surface roughness or the presence of Ru lamellas are discussed which avoid direction-sensitive measurements. A nonconducting surface barrier might account for the absence of Josephson coupling along *c*-axis oriented junctions as well.

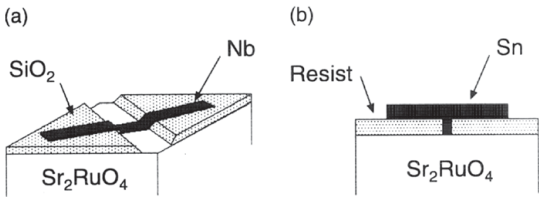

Fig. 10.12. Experimental realization of SS′ Josephson junctions on Sr_2RuO_4 (from [78])

Early SQUID experiments (see Fig. 10.11d) following the pioneering work by Kirtley and Tsuei [83] and Wollman et al. [84] on the high-temperature superconductors suffer from the reduced T_c of the junctions and the obvious surface degradation during junction preparation [80, 81]. More recently, Nelson et al. found a clear difference between the critical current in the limit of zero magnetic flux of SQUID devices with junctions on the same side of a Sr_2RuO_4 crystal (*c*-axis junction, see Fig. 10.11d) and junctions on opposite sides (in-plane junctions) [85]. They reported a maximum of $I_c(\Phi = 0)$ for the *c*-axis junction and a minimum of $I_c(\Phi)$ at $\Phi = 0$ for in-plane junctions. The result indicates that the superconducting phase changes by π under inversion and verifies odd-parity, spin-triplet pairing in Sr_2RuO_4. The position of the minimum, however, slightly deviates from $\Phi = 0$. The asymmetry of the critical current with respect to Φ was interpreted as an additional confirmation of

the chiral p-wave symmetry by Asano et al. who calculated the response of the critical Josephson current to applied magnetic fields for different types of ring topology and pairing symmetries [86].

Flux Line Lattice

Information about the vortex lattice have been obtained both by μSR measurements in the transverse field [53, 54] and by small-angle neutron scattering (SANS) [87, 88]. In the μSR experiment the time evolution of the muon polarization was measured and from the real part of the Fourier transform the probability distribution of the local fields has been obtained. The line shape of this distribution function is in good agreement with vortices forming a square lattice, at least at the applied field of 6 mT [53] and 15 mT [54]. The observation of a square lattice is not by itself a proof for non-s-wave superconductivity. The lattice structure may change as a function of field in conventional s-wave superconductors as well and a square vortex lattice can arise from non-local effects [89]. Indeed, this was experimentally observed in members of the borocarbide family RNi_2B_2C [90, 91, 92].

The presence of a square vortex lattice was confirmed by the SANS experiments [87, 88] in magnetic fields of $B = 10$, 20, and 30 mT parallel to the c-axis of Sr_2RuO_4, i. e. perpendicular to the layers. The orientation of the flux line lattice is such that the nearest-neighbour direction is at 45° to the Ru-O-Ru direction in the crystal lattice (compare with Fig. 10.2). The result was interpreted in terms of the two-component Ginzburg-Landau model for the superconductivity of Sr_2RuO_4 in presence of a magnetic field as proposed by Agterberg [93, 94]. In this model the order parameter has two components (η_1, η_2) and belongs to the two-dimensional representations Γ_{5u} of the tetragonal point group D_{4h} [60]. A time-reversal symmetry breaking state would be realized for $(\eta_1, \eta_2) \propto (1, i)$ and the orbital symmetry properties are reproduced by $k_x + ik_y$. The measured intensities of different flux lattice Bragg reflections have been shown to be in qualitative agreement with this model which describes a p-wave state. On the base of this Heeb and Agterberg calculated the vortex core structure and proposed a fourfold deformation of the vortex core which should be observable in scanning tunnelling measurements.

A certainly intriguing method was used to study the field penetration in a magnetic field applied almost within the ab plane of Sr_2RuO_4, namely μSQUID force microscopy [95]. The μSQUID force microscope consists of a piezoelectric tuning fork carrying the SQUID. By detecting the interaction forces between the SQUID tip and sample surface the magnetic flux penetrating the superconductor in the vortex state has been imaged. The images taken at low fields show the magnetic flux starting to penetrate the crystal in form of elongated flux chains, oriented along the field direction. The formation of vortex chains is driven by the transverse magnetization of the tilted vortices. The effect has already been observed for other superconductors, e. g. the high-T_c's (see Sect. 10.2).

Superconductivity Models

One possibility to deliberate on the question of the order-parameter symmetry is to look at the possible pairing states allowed under the aspects of the group theory. The possible pairing states of Sr_2RuO_4 can be classified according to the irreducible representations of the D_{4h} point group [60]. The only state which breaks time-reversal symmetry is the odd parity E_u state which can be expressed by the vector function $\boldsymbol{d}(\boldsymbol{k}) = \hat{\boldsymbol{z}}(k_x \pm ik_y)$. Other possible time-reversal symmetry breaking states would require complex combinations of states belonging to different representations which would in general lead to double superconducting transitions, with broken time reversal only below the lower transition. As there is no evidence to date of multiple superconducting transitions, the E_u state is the only one compatible with the experimental data.

Based on the proposal by Rice and Sigrist [7] that modest ferromagnetic enhancement in the Fermi liquid state favors p-wave superconductivity the earliest model assumed a p-wave order parameter in analogy to the A phase of ^{3}He, namely the unitary spin-triplet $\boldsymbol{d}(\boldsymbol{k}) = \hat{\boldsymbol{z}}(k_x \pm ik_y)$ order parameter. However, the pairing state is isotropic in the basal plane and fully gapped, which contradicts the observation of line nodes in several experiments. As shown by Blount [96] symmetry requires spin-triplet superconductors to be nodeless or have point nodes but not line nodes. Line nodes in a spin-triplet state can appear only accidentally if spin-orbit coupling is present. The proposed non-unitary p-wave model [97, 98] is incompatible with the observation of line nodes as well.

In order to account for the NMR results Miyake and Narikiyo [50] showed that starting from a pairing interaction mediated by short-range ferromagnetic spin fluctuations a modified order parameter $\boldsymbol{d}(\boldsymbol{k}) = \Delta_0\hat{\boldsymbol{z}}(\sin k_x + i \sin k_y)$ is obtained instead of the isotropic $\boldsymbol{d}(\boldsymbol{k}) = \Delta_0\hat{\boldsymbol{z}}(k_x + ik_y)$. Furthermore, the amplitude of the gap is described approximately by a fourfold-symmetry gap function of $|\boldsymbol{d}(\boldsymbol{k})| = \Delta_0[1 - r\cos(4\theta_k)]$ with $r = 0.692$. This gap function has vertical line nodes.

Hasegawa et al. [67] have proposed a phenomenological model with several possible f-wave pairing states which have been constructed from the product of two-dimensional odd-parity E_u representations with different even-parity representations which are chosen to have zeros. The stability of such mixed-parity states has been investigated by Eschrig et al. [27]. Among all states allowed by symmetry the following states are the most promising candidates for an explanation of the experimental findings of μSR, NMR and specific heat:

$$\boldsymbol{d}(\boldsymbol{k}) = \Delta_0\hat{\boldsymbol{z}}(k_x + ik_y)k_xk_y \tag{10.7}$$

$$\boldsymbol{d}(\boldsymbol{k}) = \Delta_0\hat{\boldsymbol{z}}(k_x + ik_y)(k_x^2 - k_y^2) \tag{10.8}$$

$$\boldsymbol{d}(\boldsymbol{k}) = \Delta_0\hat{\boldsymbol{z}}(k_x + ik_y)(\cos(ck_z) + a_0) \tag{10.9}$$

These are time-reversal symmetry-broken states which have line nodes running either vertically (10.7 and 10.8) or horizontally (10.9). However, only $\boldsymbol{d}(\boldsymbol{k}) = \hat{\boldsymbol{z}}\Delta_0(k_x + ik_y)(\cos(ck_z) + a_0)$ with $|a_0| < 1$ and real, can account for the θ dependence of the thermal conductivity under rotation of the magnetic field [41]. Graf

and Balatsky [26] analyzed the specific-heat data and conclude that pairing states similar to those above in 10.7 are possible. On the other hand, Wu and Joynt [99] analyzed ultrasonic-absorption and thermal-conductivity measurements and came to the conclusion that only the state in 10.8 can qualitatively account for the transport data.

Other models take into account the multi-sheet Fermi surface of Sr_2RuO_4. Won and Maki [100] assumed that the order parameter is the same for all three bands and considered a f-wave order parameter with $\boldsymbol{d}(\boldsymbol{k}) = \Delta_0 \hat{\boldsymbol{z}} k_z (k_x + ik_y)^2$. This order parameter has horizontal line nodes and can account for the observed power laws in the thermodynamic properties. The orbital-dependent superconductivity model proposed by Agterberg et al. [49] assumes that interband pairing interaction of quasiparticles is weak between the γ band characterized by the Ru $4d_{xy}$ orbitals and the α and β bands by the Ru $4d_{xz}$ and $4d_{yz}$ orbitals so that a large gap occurs on the γ band and only small proximity-induced gaps on the α and β bands. As a consequence, the ungapped Fermi surfaces can account for the residual density of states observed in early specific-heat measurements, at least until a second phase transition appears at very low T. However, the residual density of states observed in early specific-heat measurements seems not to be intrinsic and, up to now, no second phase transition has been found in zero field.

Zhitomirsky and Rice [101] extended this model in order to account for the experimental findings. They proposed that line nodes exist only on two of the three Fermi surfaces: a fully-gapped Fermi surface exists in the active γ band, which drives the superconducting transition, while line nodes develop in passive α and β bands by the interband proximity effect. They found that a nodeless axial order parameter $\boldsymbol{d}(\boldsymbol{k}) \propto (k_x + ik_y)$ in the active band can induce superconducting gaps $\boldsymbol{d}(\boldsymbol{k}) \propto (k_x + ik_y)\cos(k_z/2)$ with horizontal line nodes in the passive bands and they showed that this model almost perfectly describes the specific-heat data.

A similar approach was chosen by Nomura and Yamada [103, 104]. By solving the linearized Eliashberg equation on the basis of the two-dimensional three-band Hubbard model they determined the superconducting gap structure of Sr_2RuO_4. They showed that the momentum dependence of the effective pairing interaction on the γ band favors p-wave pairing on this band, while the pairing on the α and β

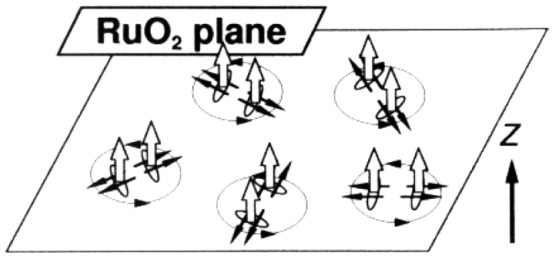

Fig. 10.13. Schematic representation of the vector order parameter $\boldsymbol{d}(\boldsymbol{k}) = \hat{\boldsymbol{z}}\Delta_0(k_x + \imath k_y)$ for Sr_2RuO_4. Small arrows depict the spins and the large arrows depict the orbital angular moments (from [102])

bands is induced through pair scattering from the γ band. Therefore, spin-triplet superconductivity in Sr_2RuO_4 is the natural result of electron correlations, and cannot considered as a result of strong magnetic correlations. Under the assumption that the orbital symmetry of the Cooper pairs is p-wave with $k_x + ik_y$ symmetry they found that the induced gap function on the β band has vertical line nodes at $k_x = \pm k_y$. With this model the specific-heat data [105] have been explained successfully. They calculated that the specific-heat jump is dominated by that of the γ band but the low-temperature thermal excitations in the superconducting state are dominated by those of the β band due to the vertical line-node-like structure. In addition, on the basis of this model the angular modulated specific-heat data have been interpreted [36, 40].

In conclusion, there is still a lot of controversy on a definite assignment of the order-parameter symmetry. But further discussion of the various models and additional excellent experiments will add more pieces to that puzzle and finally reveal a consistent picture of the pairing state of Sr_2RuO_4.

10.2 High-Temperature Superconductors

The discovery of superconductivity in the La-Ba-Cu-O system in 1986 by Bednorz and Müller [106] was like a big drumbeat in the hall of superconductivity and it opened a run of research activities into the new field of metal-oxide compounds. As already mentioned above, a common structural element of high-temperature superconductors are copper-oxide planes which dominate the superconducting properties (see Fig. 10.14). In addition, the "123" class of materials contains CuO chains which are thought to serve as a charge-carrier reservoir to control the electron density in the planes. The mobile charge carriers which reside primarily within the CuO_2 planes can be electrons, but are usually holes. Many of the cuprates can be doped with charge carriers and rendered superconducting by substitution of appropriate elements into an antiferromagnetic insulating parent compound. One well-investigated example is $YBa_2Cu_3O_{7-\delta}$ with $T_c = 93\,\mathrm{K}$ at optimal doping. The undoped parent compound $YBa_2Cu_3O_6$ is an antiferromagnetic insulator. There is still no consensus on the mechanism causing the high T_c in these materials. However, most properties can be well described within the concepts of Bardeen-Cooper-Schrieffer theory and Ginzburg-Landau theory.

As already stated in the beginnning, this book is not dedicated to review the high-temperature superconductors. There exist a vast of excellent review articles and monographs [107, 108, 109, 110, 111, 112, 113] which give a quite complete overview on the state-of-art of research on this material and which should be referred to. However, for sake of completeness and especially, to account for the importance of the research on the high-temperature superconductors for the understanding of the many properties of other unconventional superconductors, a short flash on the order-parameter symmetry and the concomitant physical properties will be given.

Nodal Structure

A very large number of experiments that probed the nodal structure showed that there exists a finite density of states all the way down to zero energy. However,

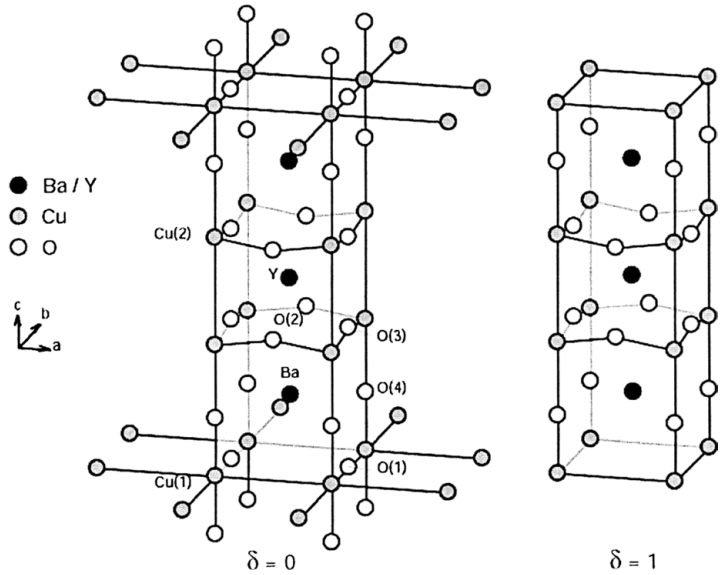

Fig. 10.14. Schematic representation of the unit cells of the crystal structure of $YBa_2Cu_3O_{7-\delta}$ for $\delta = 0$ and $\delta = 1$ (from [2])

there is limited quantitative consistency between different samples and different experimental techniques and it is not clear what is the intrinsic property. Penetration-depth measurements, for example, showed a linear temperature dependence of λ^{-2} in line with theoretical predictions for the $d_{x^2-y^2}$ gap. Measurements of the thermal conductivity at low temperature $T < 10^{-3}T_c$ (see Fig. 10.15) report a T^3 power law and a residual linear term in the thermal conductivity of both optimally doped $YBa_2Cu_3O_{7-\delta}$ and $Bi_2Sr_2CaCu_2O_8$ [114]. The magnitude of the linear term is in excellent agreement with the value expected from Fermi-liquid theory and the *d*-wave energy spectrum. This was taken as a hint that thermally excited quasiparticles are a significant mechanism in suppressing the superfluid density in cuprate superconductors.

Spin State and Parity

NMR measurements on the high-temperature superconductors showed the absence of a Hebel-Slichter peak in the relaxation rate $1/T_1$. At low temperature the relaxation rate exhibits a power law with an exponent between 3 and 4.5. Knight shift measurements involving nuclei on different lattice sites of $YBa_2Cu_3O_{7-\delta}$ show a strong reduction of K in the superconducting state which clearly reflects spin singlet pairing [116, 117]. Theoretical model calculations gave better agreement, if *d*-wave rather than *s*-wave pairing was assumed [118]. For further information on NMR measurements the review by Pennington and Slichter should be referred to [119].

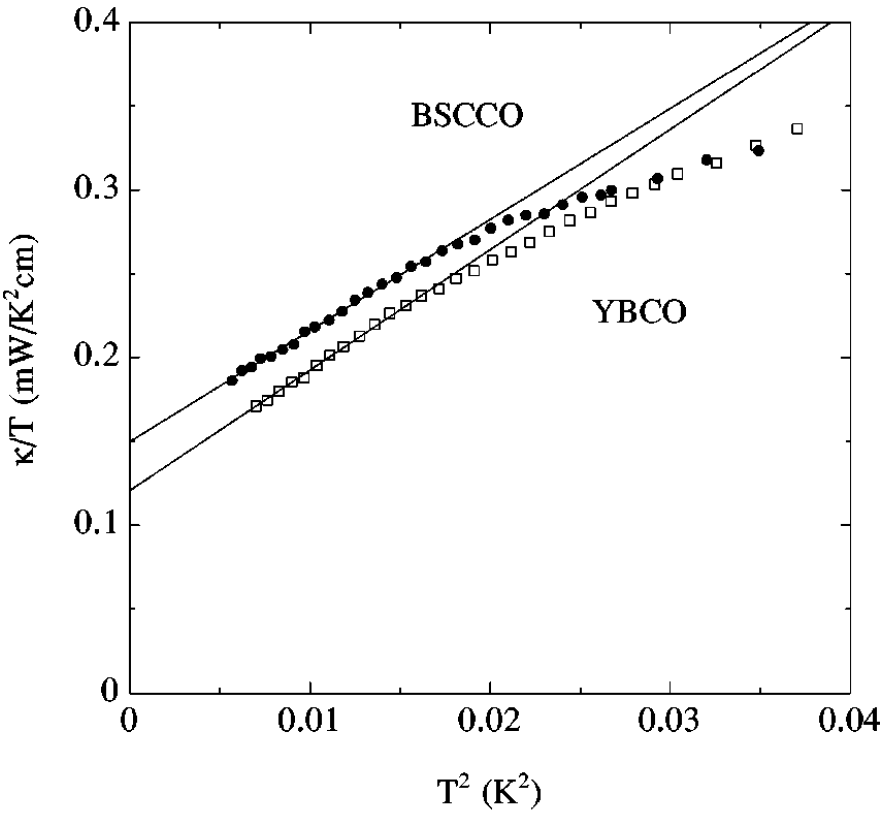

Fig. 10.15. Low-temperature thermal conductivity of $YBa_2Cu_3O_{6.9}$ and $Bi_2Sr_2CaCu_2O_8$ at optimum doping. The lines are linear fits to the data below 130 mK (from [114])

Energy Gap

There have been many experimental data reported of point-contact and tunnelling spectroscopy on high-T_c superconductors. The experimental methods that have been applied to study the electronic states range from scanning tunnelling microscopy/spectroscopy, thin-film junctions to point contacts and break junctions. A review of the tunnelling spectroscopy on high-T_c superconductors was given recently by Kashiwaya and Tanaka [120]. Most measurements of the gap width suggest considerably larger values for $2\Delta/k_BT_c$ than the BCS weak-coupling value of 3.5. For example, STM measurements by Maggio-Apprile et al. [121] found a gap width of $YBa_2Cu_3O_{7-\delta}$ of about 20 meV corresponding to $2\Delta/k_BT_c = 5.1$. Other values range between 4 and 7. A certainly exceptional test of the pairing symmetry has been reported by Wei et al. [115]. They measured tunnelling and point-contact spectra for different orientations of a $YBa_2Cu_3O_{7-\delta}$ crystal using a low-temperature scanning tunnelling microscope. For measurements on tunnel junctions with tunnelling current along the [110] direction a zero-bias anomaly has been reported

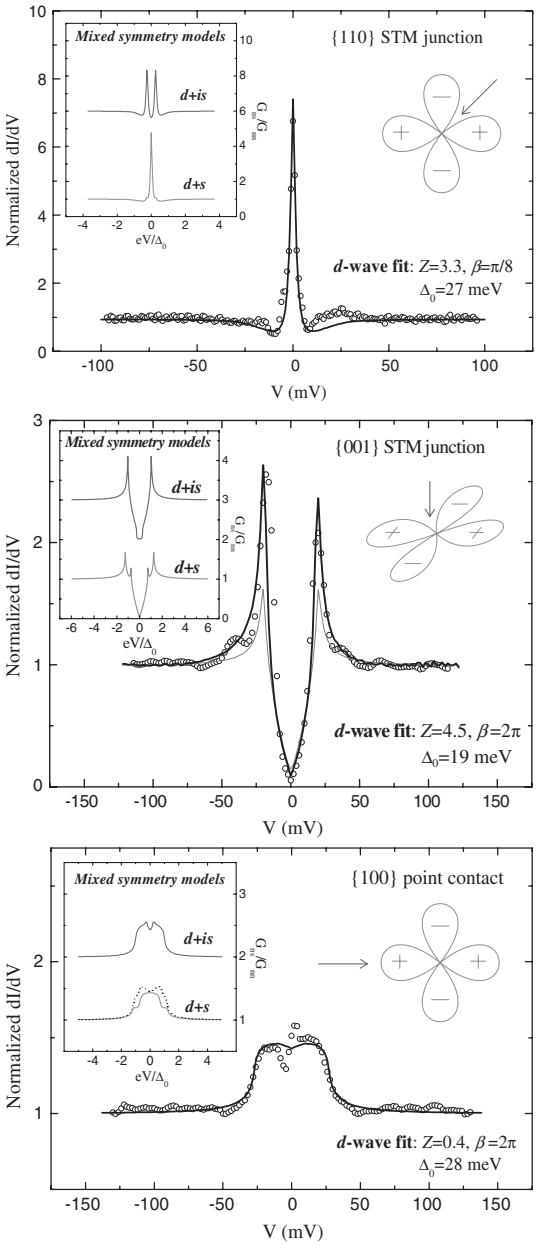

Fig. 10.16. Tunnelling spectroscopy on $YBa_2Cu_3O_{7-\delta}$ for different orientation of the crystal and different transparency of the interface. For measurements on tunnel junctions with tunnelling current along the [110] direction a zero-bias anomaly has been reported which is absent for tunnelling current along the [100] direction and for the point contact with high transparency (by courtesy of J. Wei, U Toronto)

which is absent for tunnelling current along the [100] direction and for the point contact [115]. Theoretical results for the *ab* plane tunnelling conductance by Fogelström et al. [122] have shown that a zero-bias conductance anomaly is expected if the order parameter exhibits a sign change (see Sect. 6.2). Therefore, the measurements directly prove the $d_{x^2-y^2}$ symmetry of the order parameter.

Phase-Sensitive Experiments

Although supported by many experiments, the $d_{x^2-y^2}$ symmetry of the order parameter has definitely assigned only by phase-sensitive experiments as previously suggested by Sigrist and Rice [123]. The pioneering experiments were carried out by Wollman et al. [124], who compared the SQUID characteristics of two configurations either involving a π junction either without a π junction in the SQUID loop (see Figs. 10.17 and 6.2). They found the expected shift by $\phi_0/2$ in the response to an externally applied flux (see Fig. 10.18). However, the SQUID experiments had a number of complicating factors in their interpretation. For example, twinning effects, flux trapping, demagnetization, and field-focusing effects can strongly effect the data and there has been some controversy on the interpretation of the data [126, 127, 128].

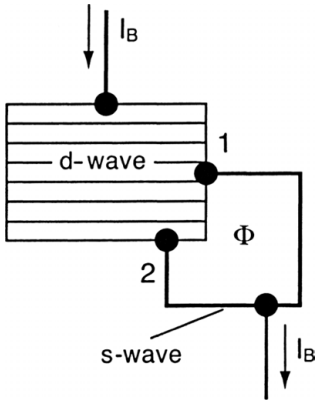

Fig. 10.17. Scheme of a SQUID-type loop for a phase-sensitive test of the order-parameter symmetry (from [123])

The possibility of errors from undetected stray trapped flux was addressed in subsequent experiments by Tsuei et al. [129] and Mathai et al. [126]. Both experiments used a scanning SQUID microscope to measure trapped flux in a ring. Mathai et al. found half-quanta of trapped flux in rings where both junctions were on different faces of a $YBa_2Cu_3O_{7-\delta}$ crystal, while there was an integral number of quanta for both junctions on the same face of the crystal. The experiment of Tsuei et al. compared three-junction and two-junction rings in a $YBa_2Cu_3O_{7-\delta}$ film (see Fig. 10.19, upper panel), finding half-integer numbers of flux quanta in the three-junction configuration and integer numbers in the two-junction rings (see Fig. 10.19, lower

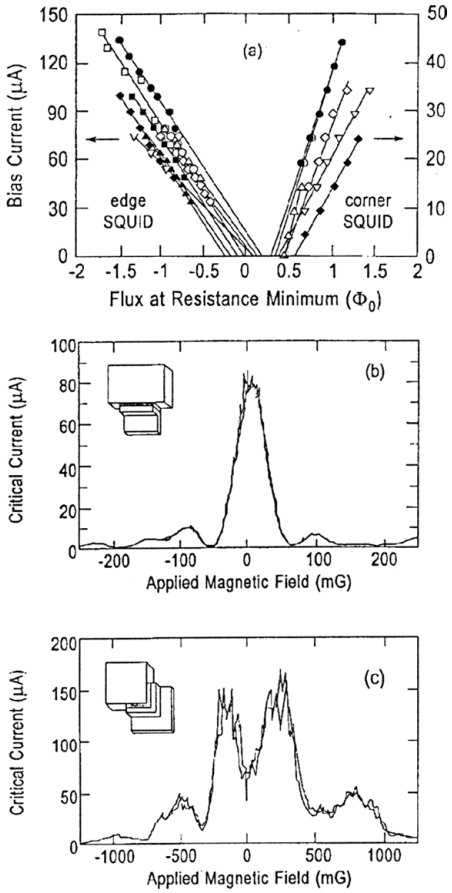

Fig. 10.18. Summary of the experimental result of Wollman et al. [124, 125]: (**a**) Extrapolation of the measured SQUID resistance minimum vs flux to zero-bias current for a corner SQUID and an edge SQUID on the same sample; (**b**) Measured critical current vs applied magnetic field for an edge junction and (**c**) for a corner junction (from [83])

panel). All of these results provide strong support for the correctness of *d*-wave pairing. The tricrystal experiment has also applied to other high-temperature superconductors. A review on the phase-sensitive experiments can be found in [83, 84]. All these experiments indicate dominant *d*-wave pairing.

Flux Line Lattice

Various techniques have been applied to high-temperature superconductors to reveal information on the flux line lattice. For fields applied parallel to the *c* axis a weakly distorted Abrikosov flux lattice has been reported [130, 131]. The distortion arises from a small in-plane effective mass anisotropy. Besides the classical Bitter decoration studies the scanning tunnelling microscope has been the main tool for such

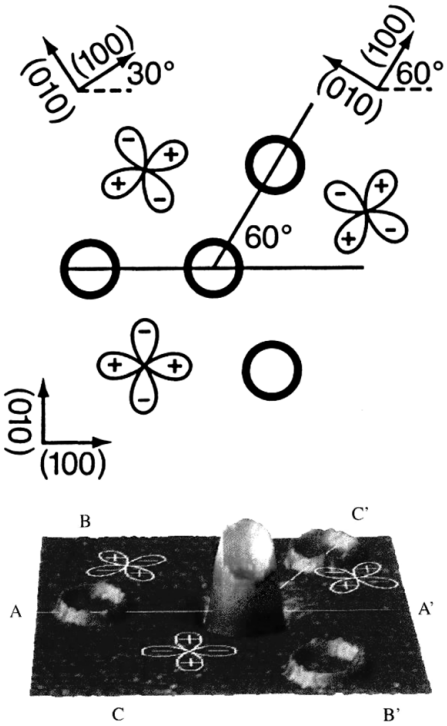

Fig. 10.19. *Upper panel*: Tricrystal geometry and ring orientation of the Scanning-SQUID experiment by Tsuei et al.. The central, three-junction ring should be a π ring for $d_{x^2-y^2}$ pairing (from [129]). *Lower panel*: Three-dimensional image of a thin-film $YBa_2Cu_3O_{7-\delta}$ tricrystal ring sample, cooled and imaged in nominally zero field. The outer rings have no flux, the central three-junction ring has half of a flux quantum spontaneously generated (from [83])

investigations. Both methods revealed a vortex chain state [132, 133] in tilted fields. For $YBa_2Cu_3O_{7-\delta}$ the vortex lattice is transformed into a pinstripe array of vortex chains, oriented to lie in the plane defined by B and c [132]. As the applied field is increased, the chains merge smoothly into an isotropic vortex lattice, still oriented in the same direction.

Most attention have attracted studies of the electronic structure of the vortex cores. Bound quasiparticle states can exist inside the vortex cores with lowest energy given approximately by $E \propto \Delta^2/2E_F$, where E_F is the Fermi energy and Δ is the superconducting gap. Vortex core states have been identified for $YBa_2Cu_3O_{7-\delta}$ by Maggio-Aprile et al. [121] and for $Bi_2Sr_2CaCu_2O_8$ by Pan et al. [20]. However, a fourfold symmetry sometimes predicted for d-wave vortices was not seen in the latter experiment. This was explained by quasiparticle states bound in the vortex cores whose order parameter is locally nodeless due to the presence of a magnetic field.

References

1. A. Schilling, M. Cantoni, J.D. Guo, H.R. Ott: Nature **363**, 56 (1993) 121
2. H.R. Ott: *The physics of superconductors*, Vol. I. Conventional and high-T_c superconductors (Springer, 2003), Chap. 6 High-T_c superconductors, p. 385 121, 141
3. P.B. Allen, H. Berger, O. Chauvet, L. Forro, T. Jarlborg, A. Junod, B. Revaz, G. Santi: Phys. Rev. B **53**(8), 4393 (1996) 122
4. L. Klein, J.S. Dodge, C.H. Ahn, J.W. Reiner, L. Mieville, T.H. Geballe, M.R. Beasley, A. Kapitulnik: J. Phys.: Condens. Matter **8**, 10 111 (1996) 122
5. R.S. Perry, L.M. Galvin, S.A. Grigera, L. Capogna, A.J. Schofield, A.P. Mackenzie, M. Chiao, S.R. Julian, S.I. Ikeda, S. Nakatsuji, Y. Maeno, C. Pfleiderer: Phys. Rev. Lett. **86**(12), 2661 (2001) 122
6. Y. Maeno, T.M. Rice, M. Sigrist: Physics Today **54**(1), 42 (2001) 122
7. T.M. Rice, M. Sigrist: J. Phys.: Condens. Matter **7**(47), L643 (1995) 6, 122, 138
8. A.P. Mackenzie, S.R. Julian, A.J. Diver, G.J. McMullan, M.P. Ray, G.G. Lonzarich, Y. Maeno, S. NishiZaki, T. Fujita: Phys. Rev. Lett. **76**, 3786 (1996) 122
9. C. Bergemann, S.R. Julian, A.P. Mackenzie, S. NishiZaki, Y. Maeno: Phys. Rev. Lett. **84**(12), 2662 (2000) 122
10. C. Bergemann, A.P. Mackenzie, S.R. Julian, D. Forsythe, E. Ohmichi: Adv. Phys. **52**(7), 639–725 (2003) 122
11. T. Imai, A.W. Hunt, K.R. Thurber, F.C. Chou: Phys. Rev. Lett. **81**, 3006 (1998) 123
12. Y. Sidis, M. Braden, P. Bourges, B. Hennion, S. NishiZaki, Y. Maeno, Y. Mori: Phys. Rev. Lett. **83**, 3320 (1999) 123
13. F. Servant, B. Fåk, S. Raymond, J.P. Brison, P. Lejay, J. Flouquet: Phys. Rev. B **65**, 184 511 (2002) 123
14. I.I. Mazin, D.J. Singh: Phys. Rev. Lett. **82**(21), 4324 (1999) 123
15. N. Kikugawa, A.P. Mackenzie, Y. Maeno: J. Phys. Soc. Jpn. **72**(2), 237–240 (2003). (see also cond-mat/0210190) 123
16. N. Kikugawa, S. Saita, M. Minakata, Y. Maeno: Physica B **312-313**, 803 (2002) 123
17. A.P. Mackenzie, R.K.W. Haselwimmer, A.W. Tyler, G.G. Lonzarich, Y. Mori, S. NishiZaki, Y. Maeno: Phys. Rev. Lett. **80**, 161 (1998) 123
18. Z.Q. Mao, Y. Mori, Y. Maeno: Phys. Rev. B **60**, 610 (1999) 123
19. J.B. Kycia, J.I. Hong, M.J. Graf, J.A. Sauls, D.N. Seidman, W.P. Halperin: Phys. Rev. B **58**(2), R603 (1998) 91, 123
20. S.H. Pan, E.W. Hudson, K.M. Lang, H. Eisaki, S. Uchida, J.C. Davis: Nature **403**, 746–750 (2000) 123, 146
21. A.A. Abrikosov, L.P. Gor'kov: Zh. Eksp. Teor. Fiz. **39**(6), 1781 (1960). (Sov. Phys. JETP **12**, 1243 (1961)) 123
22. A.J. Millis, S. Sachdev, C.M. Varma: Phys. Rev. B **37**(10), 4975 (1988) 123, 133
23. R.J. Radtke, K. Levin, H.B. Schüttler, M.R. Norman: Phys. Rev. B **48**(1), 653 (1993) 123
24. C. Honerkamp, M. Sigrist: J. Low Temp. Phys. **111**(516), 895 (1998) 123, 133
25. M. Sigrist, D. Agterberg, A. Furusaki, C. Honerkamp, K.K. Ng, T.M. Rice, M.E. Zhitomirski: Physica C **317-318**, 134 (1999) 123, 133
26. M.J. Graf, A.V. Balatsky: Phys. Rev. B **62**, 9697 (2000) 123, 125, 139
27. M. Eschrig, J. Ferrer, M. Fogelström: Phys. Rev. B **63**, 220 509(R) (2001) 123, 138
28. H. Kusunose, M. Sigrist: Europhys. Lett. **60**, 281 (2002) 123, 125
29. R. Werner: Phys. Rev. B **67**, 014 505 (2003) 123
30. G. Baskaran: Physica B **223 & 224**, 490 (1996) 6, 123

31. I. Eremin, D. Manske, K.H. Bennemann: Phys. Rev. B **65**, 220 502(R) (2002). (see also cond-mat/0202051) 123
32. A.A. Ovchinnikov, M.Y. Ovchinnikova: cond-mat/0205529 (2002) 123
33. A.P. Mackenzie, Y. Maeno: Rev. Mod. Phys. **75**(2), 657–712 (2003) 123
34. S. NishiZaki, Y. Maeno, S. Farner, S. Ikeda, T. Fujita: J. Phys. Soc. Jpn. **67**, 560 (1998) 123, 155
35. C. Langhammer, F. Steglich, M. Lang, T. Sasaki: Eur. Phys. J. B **26**, 413–416 (2002) 123, 155
36. K. Deguchi, Z.Q. Mao, Y. Maeno: J. Phys. Soc. Jpn. **73**(5), 1313–1321 (2004). (see also cond-mat/0404070v2) 124, 125, 140, 155
37. I. Vekhter, P.J. Hirschfeld, J.P. Carbotte, E.J. Nicol: Phys. Rev. B **59**(14), R9023 (1999) 22, 124
38. H. Won, K. Maki: cond-mat/0004105 (2000) 22, 124
39. H. Won, K. Maki: Europys. Lett. **56**(5), 729–735 (2001) 124
40. K. Deguchi, Z.Q. Mao, H. Yaguchi, Y. Maeno: Phys. Rev. Lett. **92**(4), 047 002 (2004) 124, 140, 155
41. K. Izawa, H. Takahashi, H. Yamaguchi, Y. Matsuda, M. Suzuki, T. Sasaki, T. Fukase, Y. Yoshida, R. Settai, Y. Onuki: Phys. Rev. Lett. **86**, 2653 (2001) 75, 125, 138, 155
42. H. Suderow, J.P. Brison, J. Flouquet, A. Tyler, Y. Maeno: J. Phys. Cond. Matt. **10**(34), L597 (1998) 93, 125, 154, 155
43. M. Suzuki, M.A. Tanatar, N. Kikugawa, Z.Q. Mao, Y. Maeno, T. Ishiguro: Phys. Rev. Lett. **88**, 227 004 (2002) 125, 155
44. M.A. Tanatar, S. Nagai, Z.Q. Mao, Y. Maeno, T. Ishiguro: Physica C **341-348**(3), 1841 (2000) 125, 155
45. M.J. Graf, S.K. Yip, J.A. Sauls: J. Low Temp. Phys. **102**(516), 367 (1996) 22, 74, 75, 91, 92, 93, 125
46. M.E. Zhitomirsky, M.B. Walker: Phys. Rev. B **57**(14), 8560 (1998) 125
47. M.A. Tanatar, M. Suzuki, S. Nagai, Z.Q. Mao, Y. Maeno, T. Ishiguro: Phys. Rev. Lett. **86**, 2649 (2001) 125, 155
48. I. Bonalde, B.D. Yanoff, M.B. Salamon, D.J. Van Harlingen, E.M.E. Chia, Z.Q. Mao, Y. Maeno: Phys. Rev. Lett. **85**, 4775 (2000) 125, 155
49. D.F. Agterberg, T.M. Rice, M. Sigrist: Phys. Rev. Lett. **78**, 3374 (1997) 125, 139
50. K. Miyake, O. Narikiyo: Phys. Rev. Lett. **83**, 1423 (1999) 125, 128, 138
51. P.J. Hirschfeld, N. Goldenfeld: Phys. Rev. B **48**(6), 4219 (1993) 24, 75, 125
52. I. Kosztin, A.J. Leggett: Phys. Rev. Lett. **79**(1), 135 (1997) 75, 125
53. C.M. Aegerter, S.H. Lloyd, C. Ager, S.L. Lee, S. Romer, H. Keller, E.M. Forgan: J. Phys.: Condens. Matter **10**(33), 7445 (1998) 126, 137, 155, 161
54. G.M. Luke, Y. Fudamoto, K.M. Kojima, M.I. Larkin, B. Nachumi, Y.J. Uemura, J.E. Sonier, Y. Maeno, Z.Q. Mao, Y. Mori, D.F. Agterberg: Physica B **289-290**, 373 (2000) 126, 137, 155, 157, 161
55. P. Contreras, M. Walker, K. Samokhin: Phys. Rev. B **70**, 184 528 (2004). (see also cond-mat/0407181v1) 126, 127
56. C. Lupien, W.A. MacFarlane, C. Proust, L. Taillefer, Z.Q. Mao, Y. Maeno: Phys. Rev. Lett. **86**(26), 5986 (2001). (see also cond-mat/0101319) 126, 127, 155
57. H. Matsui, Y. Yoshida, A. Mukai, R. Settai, Y. Onuki, H. Takei, N. Kimura, H. Aoki, N. Toyota: Phys. Rev. B **63**, 060 505(R) (2001) 126, 155
58. J.D. Gavenda: Phys. Rev. B **66**, 216 501 (2002) 126
59. G.M. Luke, Y. Fundamoto, K.M. Kojima, M.I. Larkin, J. Merrin, B. Nachumi, Y.J. Uemura, Y. Maeno, Z.Q. Mao, Y. Mori, H. Nakamura, M. Sigrist: Nature **394**, 558 (1998) 127, 157
60. M. Sigrist, K. Ueda: Rev. Mod. Phys. **63**(2), 239 (1991) 11, 14, 17, 29, 50, 61, 90, 100, 128, 137, 138
61. Y. Okuno, M. Matsumoto, M. Sigrist: J. Phys. Soc. Jpn. **68**(9), 3054 (1999) 128
62. G.M. Luke, A. Keren, L.P. Le, W.D. Wu, Y.J. Uemura, D.A. Bonn, L. Taillefer, J.D. Garrett: Phys. Rev. Lett. **71**, 1466 (1993) 91, 94, 96, 128, 156
63. K. Ishida, H. Mukuda, Y. Kitaoka, K. Asayama, Z.Q. Mao, Y. Mori, Y. Maeno: Nature **396**, 658 (1998) 128, 157

64. K. Ishida, H. Mukuda, Y. Kitaoka, Z.Q. Mao, H. Fukazawa, Y. Maeno: Phys. Rev. B **63**, 060 507(R) (2001) 128, 157
65. H. Murakawa, K. Ishida, K. Kitagawa, Z.Q. Mao, Y. Maeno: Phys. Rev. Lett. **93**(16), 167 004 (2004) 29, 128, 157
66. K. Ishida, Y. Kitaoka, K. Asayama, S. Ikeda, S. Nishizaki, Y. Maeno, K. Yoshida, T. Fujita: Phys. Rev. B **56**(2), R505 (1997) 128, 157
67. Y. Hasegawa, K. Machida, M. Ozaki: J. Phys. Soc. Jpn. **69**, 336 (2000) 128, 138
68. H. Mukuda, K. Ishida, Y. Kitaoka, K. Miyake, Z.Q. Mao, Y. Mori, Y. Maeno: Phys. Rev. B **65**, 132 507 (2002) 128, 157
69. F. Laube, G. Goll, H. v. Löhneysen, M. Fogelström, F. Lichtenberg: Phys. Rev. Lett. **84**, 1595 (2000) 129, 132, 133, 159
70. R. Jin, Y. Zadorozhny, Y. Liu, D.G. Schlom, Y. Mori, Y. Maeno: Phys. Rev. B **59**, 4433 (1999) 129, 130, 135, 159, 160
71. M.D. Upward, L.P. Kouwenhoven, A.F. Morpurgo, N. Kikugawa, Z.Q. Mao, Y. Maeno: Phys. Rev. B **65**, 220 512(R) (2002) 129, 130, 159
72. W.L. McMillan, J.M. Rowell: *Tunneling and strong-coupling superconductivity* (Marcel Dekker, Inc., New York, 1969), p. 561 36, 129
73. F. Laube, G. Goll, H. v. Löhneysen, F. Lichtenberg: J. Low Temp. Phys. **117**(516), 1575 (1999) 131, 159
74. I.O. Kulik: Sov. J. Low Temp. Phys. **18**, 302 (1992) 41, 42, 43, 131
75. G.E. Blonder, M. Tinkham, T.M. Klapwijk: Phys. Rev. B **25**, 4515 (1982) 44, 45, 49, 51, 78, 99, 133
76. F. Laube, G. Goll, M. Eschrig, M. Fogelström, R. Werner: Phys. Rev. B **69**, 014 516 (2004). (see also cond-mat/0301221) 50, 51, 52, 133, 159
77. F. Laube, G. Goll, H. v. Löhneysen, F. Lichtenberg: submitted for publication (2005) 135
78. A. Sumiyama, T. Endo, Y. Oda, Y. Yoshida, A. Mukai, A. Ono, Y. Ōnuki: Physica C **367**, 129 (2002) 135, 136, 160
79. R. Jin, Y. Liu, Z.Q. Mao, Y. Maeno: Europhys. Lett. **51**, 341 (2000) 135, 136, 160
80. Y. Liu, K.D. Nelson, Z.Q. Mao, R. Jin, Y. Maeno: J. Low Temp. Phys. **131**(5-6), 1059–1068 (2003) 135, 136, 159, 160
81. K.D. Nelson, Z.Q. Mao, Y. Maeno, Y. Liu: Physica C **388-389**, 491–492 (2003) 135, 136, 160
82. C. Honerkamp, M. Sigrist: Prog. Theor. Phys. **100**(1), 53 (1998) 135
83. C.C. Tsuei, J.R. Kirtley: Rev. Mod. Phys. **72**(4), 969 (2000) 5, 136, 145, 146
84. D.J. Van Harlingen: Rev. Mod. Phys. **67**(2), 515 (1995) 58, 136, 145
85. K.D. Nelson, Z.Q. Mao, Y. Maeno, Y. Liu: Science **306**, 1151–1154 (2004) 136, 160
86. Y. Asano, Y. Tanaka, M. Sigrist, S. Kashiwaya: Phys. Rev. B **71**, 214 501 (2005) 137
87. T.M. Riseman, P.G. Kealey, E.M. Forgan, A.P. Mackenzie, L.M. Galvin, A.W. Tyler, S.L. Lee, C. Ager, D.M. Paul, C.M. Aegerter, R. Cubitt, Z.Q. Mao, T. Akima, Y. Maeno: Nature **396**, 242 (1998). Correction, *ibid* **404**, 629 (2000) 137, 161
88. P.G. Kealey, T.M. Riseman, E.M. Forgan, L.M. Galvin, A.P. Mackenzie, S.L. Lee, D.M. Paul, R. Cubitt, D.F. Agterberg, R. Heeb, Z.Q. Mao, Y. Maeno: Phys. Rev. Lett. **84**, 6094 (2000) 137, 161
89. V.G. Kogan, M. Bullock, B. Harmon, P. Miranović, L. Dobrosavljević-Grujić, P.L. Gammel, D.J. Bishop: Phys. Rev. B **55**(14), R8693 (1997) 137
90. M.R. Eskildsen, P.L. Gammel, B.P. Barber, U. Yaron, A.P. Ramirez, D.A. Huse, D.J. Bishop, C. Bolle, C.M. Lieber, S. Oxx, S. Sridhar, N.H. Andersen, K. Mortensen, P.C. Canfield: Phys. Rev. Lett. **78**(10), 1968 (1997) 6, 137
91. D.M. Paul, C.V. Tomy, C.M. Aegerter, R. Cubitt, S.H. Lloyd, E.M. Forgan, S.L. Lee, M. Yethiraj: Phys. Rev. Lett. **80**(7), 1517 (1998) 137
92. Y. de Wilde, M. Iavarone, U. Welp, V. Metlushko, A.E. Koshelev, I. Aranson, G.W. Crabtree. P.C. Canfield: Phys. Rev. Lett. **78**(22), 4273 (1997) 137

93. D.F. Agterberg: Phys. Rev. Lett. **80**, 5184 (1998) 137
94. D.F. Agterberg: Phys. Rev. B **58**(21), 14 484 (1998) 137
95. V.O. Dolocan, C. Veauvy, Y. Liu, F. Servant, P. Lejay, D. Mailly, K. Hasselbach: Physica C **404**, 140–144 (2004) 137, 161
96. E.I. Blount: Phys. Rev. B **32**(5), 2935 (1985) 138
97. K. Machida, M. Ozaki, T. Ohmi: J. Phys. Soc. Jpn. **65**, 3720 (1996) 138
98. M. Sigrist, M.E. Zhitomirsky: J. Phys. Soc. Jpn. **65**, 3452 (1996) 138
99. W.C. Wu, R. Joynt: Phys. Rev. B **64**, 100 507(R) (2001) 139
100. H. Won, K. Maki: cond-mat/0006151 (2000) 139
101. M.E. Zhitomirsky, T.M. Rice: Phys. Rev. Lett. **87**, 057 001 (2001) 139
102. Y. Maeno, Z.Q. Mao, S. NishiZaki, T. Akima: Physica B **280**(1-4), 285–289 (2000) 139
103. T. Nomura, K. Yamada: J. Phys. Soc. Jpn. **71**(8), 1993–2004 (2002). (see also cond-mat/0203453) 139
104. T. Nomura, K. Yamada: J. Phys. Soc. Jpn. **71**(2), 404–407 (2002) 139
105. S. NishiZaki, Y. Maeno, Z.Q. Mao: J. Phys. Soc. Jpn. **69**, 572 (2000) 140, 155
106. J.G. Bednorz, K.A. Müller: Z. Phys. B **64**, 189 (1986) 140
107. A.V. Chubukov, D. Pines, J. Schmalian: *The physics of superconductors*, Vol. 1: Conventional and High-Tc Superconductors (Springer, 2003), Chap. 7, *A Spin Fluctuation Model for d-wave Superconductivity*, p. 495 6, 140
108. E.W. Carlson, V.J. Emery, S.A. Kivelson, D. Orgad: *The physics of superconductors*, Vol. 2: Superconductivity in Nanostructures, High-T_c and Novel Superconductors, Organic Superconductors (Springer, 2003), Chap. 6, *Concepts in High Temperature Superconductivity*, p. 275 6, 140
109. M.B. Maple: J. Magn. Magn. Mater. **177**(1), 18 (1998) 6, 140
110. J. Klamut, B.W. Veal, B.M. Dabrowski, P.W. Klamut, M. Kazimierski: *Recent Developments in High Temperature Superconductors* (Springer, 1996) 6, 140
111. N.M. Plakida: *High-Temperature Superconductors* (Springer, 1995) 6, 140
112. C.P. Poole Jr., H.A. Farach, R.J. Creswick: *Superconductivity* (Academic Press, San Diego, 1995) 6, 140
113. K.H. Bennemann, J.B. Ketterson: *The physics of superconductors*, Vol. I. Conventional and high-T_c superconductors (Springer, 2003), Chap. 1 History of Superconductivity: Conventional, High-Transition Temperature and Novel Superconductors, p. 1 140
114. M. Chiao, R.W. Hill, C. Lupien, L. Taillefer, P. Lambert, R. Gagnon, P. Fournier: Phys. Rev. B **62**(5), 3554 (2000) 141, 142
115. J.Y.T. Wei, N.C. Yeh, D.F. Garrigus, M. Strasik: Phys. Rev. Lett. **81**, 2542 (1998) 144
116. S.E. Barrett, D.J. Durand, C.H. Pennington, C.P. Slichter, T.A. Friedmann, J.P. Rice, D.M. Ginsberg: Phys. Rev. B **41**, 6283 (1990) 141
117. M. Takigawa, P.C. Hammel, R.H. Heffner, Z. Fisk: Phys. Rev. B **39**, 7371 (1989) 141
118. D.J. Scalapino: Phys. Rep. **250**(6), 329 (1995) 6, 141
119. C.H. Pennington, C.P. Slichter: *Nuclear Resonance Studies of YBCO* (World Scientific, 1990), p. 269 141
120. S. Kashiwaya, Y. Tanaka: Rep. Prog. Phys. **63**(10), 1641 (2000) 142
121. I. Maggio-Aprile, C. Renner, A. Erb, E. Walker, Ø. Fischer: Phys. Rev. Lett. **75**(14), 2754–2757 (1995) 62, 142, 146
122. M. Fogelström, D. Rainer, J.A. Sauls: Phys. Rev. Lett. **79**(2), 281 (1997). E: Phys. Rev. Lett. **79**, 2754 (1997) 36, 59, 79, 144
123. M. Sigrist, T.M. Rice: J. Phys. Soc. Jpn. **61**(12), 4283 (1992) 144
124. D.A. Wollman, D.J. Van Harlingen, W.C. Lee, D.M. Ginsberg, A.J. Leggett: Phys. Rev. Lett. **71**(13), 2134 (1993) 58, 144, 145

125. D.A. Wollman, D.J. Van Harlingen, J. Giapintzakis, D.M. Ginsberg: Phys. Rev. Lett. **74**(5), 797 (1995) 80, 145
126. A. Mathai, Y. Gim, R.C. Black, A. Amar, F.C. Wellstood: Phys. Rev. Lett. **74**(22), 4523 (1995) 144
127. R.A. Klemm: Phys. Rev. Lett. **73**(13), 1871 (1994) 144
128. D.A. Wollman, D.J. van Harlingen, A.J. Leggett: Phys. Rev. Lett. **73**(13), 1872 (1994) 144
129. C.C. Tsuei, J.R. Kirtley, C.C. Chi, L.S. Yu-Jahnes, A. Gupta, T. Shaw, J.Z. Sun, M.B. Ketchen: Phys. Rev. Lett. **73**(4), 593 (1994) 58, 144, 146
130. D.J. Bishop, P.L. Gammel, D.A. Huse, C.A. Murray: Science **255**(5041), 165–172 (1992) 145
131. G.J. Dolan, F. Holtzberg, C. Feild, T.R. Dinger: Phys. Rev. Lett. **62**(18), 2184 (1989) 145
132. P.L. Gammel, D.J. Bishop, J.P. Rice, D.M. Ginsberg: Phys. Rev. Lett. **68**(22), 3343–3346 (1992) 146
133. A. Grigorenko, S. Bending, T. Tamegai, S. Ooi, M. Henini: Nature **414**, 728–731 (2001) 146